CLEAN
Soil Air Water

Reda M. Mohamed[1,2,3]
Elham S. Aazam[1]

[1]Chemistry Department, Faculty of Science, King Abdulaziz University, Jeddah, Saudi Arabia
[2]Nanostructured Material Division Advanced Materials Department, Central Metallurgical R&D Institute, Helwan, Cairo, Egypt
[3]Center of Excellence in Environmental Studies, King Abdulaziz University, Jeddah, Saudi Arabia

Research Article

New Visible-Light Pt/PbS Nanoparticle Photocatalysts for the Photocatalytic Oxidation of Thiophene

PbS nanoparticles were prepared using a hydrothermal route, and Pt was deposited onto the PbS nanoparticles via a photo-assisted deposition route. The photocatalytic performances of the PbS and Pt/PbS samples were examined for the photocatalytic oxidation of thiophene under visible light. Deposition of Pt onto the surface of PbS led to a shift in the absorption of PbS to a higher wavelength (red shift). The 0.15 wt% Pt/PbS nanoparticles had the highest photocatalytic efficiency % (100%) for the degradation of thiophene under visible light after 40 min of reaction time. The 0.15 wt% Pt/PbS nanoparticles can be used six times for the degradation of thiophene without a loss of photocatalytic activity.

Keywords: Oil pollution; Photo-assisted deposition; Photostability; Visible photocatalysts

Received: February 9, 2014; *revised:* March 2, 2014; *accepted:* March 28, 2014

DOI: 10.1002/clen.201400115

1 Introduction

The removal of dangerous organic pollutants by photocatalysis is of great importance and interest for environmental safety [1–5]. It is difficult to remove pollutants from fuel oils that contain sulfur-containing organic compounds [6]. One of the main compounds in oil pollutants is thiophene, which is very difficult to remove by a conventional oxidation process such as the desulfurization process. The low electron density on the sulfur atom and the aromaticity of the thiophene molecule make it difficult to oxidize. Therefore, researchers must develop an efficient photocatalyst to oxidize thiophene. The efficiency of the photocatalyst depends on its stability, particle size, surface area, band gap, and electron–hole recombination lifetime [7]. Many researchers have tried to develop photocatalysts by changing preparation methods, doping with metals, and oxide mixing [8–12]. The most famous photocatalyst is TiO_2, which has a band gap of approximately 3.2 eV, and many published papers have attempted to increase its photocatalytic activity and surface area and increase its e–h recombination lifetime and band gap [13–19]. The semiconductor silver sulfide has a narrow band gap with excellent optical properties and good chemical stability [20–24]. Silver sulfide has been prepared by many methods, such as using organometallic precursors [25], using gamma irradiation [26], sonochemical methods [27], templating methods [28], sol–gel and ion-implantation techniques [29], microemulsions [30], etc. To the best of our knowledge, there are no published papers about enhancement of photocatalytic activity of lead sulfide. In this work, PbS and Pt/PbS nanoparticles were prepared and characterized. The photocatalytic performance of PbS and Pt/PbS nanoparticles was studied for the oxidation of thiophene under visible light.

Correspondence: Professor R. M. Mohamed, Chemistry Department, Faculty of Science, King Abdulaziz University, Jeddah 21589, P.O. Box 80203, Saudi Arabia
E-mail: mhmdouf@gmail.com

Abbreviations: **BET**, Brunauer–Emmett–Teller; **PAD**, photo-assisted deposition; **PL**, photoluminescence; **TEM**, transmission electron microscopy; **XPS**, X-ray photoelectron spectroscopy; **XRD**, X-ray diffraction

2 Experimental

2.1 Synthesis of PbS

All chemicals used are of analytical grade and are used without further purification. The PbS nanoparticles were prepared by the following procedure. 10 mM thioacetamide and 2.5 mM $PbCl_2$ were dissolved in deionized water (40 mL). The resulting mixture was placed into an autoclave for 24 h at 200°C. The material produced was separated by centrifugation and then washed several times by deionized water and absolute ethanol. Finally, the PbS nanoparticles were dried in a vacuum oven for 3 h at 80°C.

2.2 Synthesis of Pt/PbS

The Pt/PbS nanoparticles were prepared by the photo-assisted deposition (PAD) method according to the following procedure. A certain amount of PbS was dispersed in an aqueous solution of H_2PtCl_6, and then the resulting mixture was irradiated by UV light for 24 h. The material produced was dried for 24 h at 100°C. Using the PAD method, various wt% values of Pt (0.05, 0.10, 0.15, and 0.20 wt% of Pt metal) were deposited onto the PbS.

2.3 Characterization techniques

X-ray diffraction (XRD) analysis was performed at room temperature (Bruker AXS D8) using Cu $K\alpha$ radiation ($\lambda = 1.540$ Å). The specific surface area was calculated from measurements of the N_2 adsorption using a Nova 2000-series Chromatech apparatus at

CLEAN Soil Air Water

77 K. Prior to the measurements, all of the samples were held under vacuum at 250°C for 2 h. The band gap for each of the samples was identified by UV–Vis diffuse reflectance spectra. The measurements were taken in air at room temperature over the wavelength range of 200–800 nm using UV/Vis/near IF spectrophotometry (V-570, JASCO, Japan). The transmission electron microscopy (TEM) was recorded with a JEOL-JEM-1230 microscope. The samples were prepared by suspension in ethanol and ultrasonication for 30 min. Subsequently, a small amount of this solution was placed onto a carbon-coated copper grid before it was dried and loaded into the TEM. X-ray photoelectron spectroscopy (XPS) studies were performed (Thermo Scientific K-ALPHA, XPS, England) and photoluminescence (PL) emission spectra were recorded with a Shimadzu RF-5301 fluorescence spectrophotometer.

2.4 Photoreaction apparatus and procedure

The photocatalytic oxidation reactions of thiophene were performed in a Pyrex reaction cell with O_2 bubbled in a constant flow as the oxidant. The required amount of photocatalyst was dispersed in an acetonitrile solution containing thiophene ($[\text{sulfur content}]_{\text{initial}} = 600$ ppm). The suspension was stirred in the dark for 30 min to establish adsorption/desorption equilibrium between the solution and the photocatalyst, before being irradiated by a 500-W xenon lamp with a maximum emission at approximately 470 nm, used as a source of visible light. The wavelength of the visible light was controlled by a cut-off filter ($\lambda > 420$ nm). The temperature of the reaction solution was maintained at 12°C by a flow of cooling water. The products and by-products were analyzed by GC equipped with a flame photometric detector (Agilent 7890, FED column) and gas chromatography–mass spectrometry after the catalyst particles had been separated from the reaction system by centrifugation. The chromatographic conditions applied for the photocatalytic oxidation of thiophene are summarized in Tab. 1.

3 Results & Discussion

3.1 Morphological, structural and compositional characterization

Figure 1 shows the XRD patterns of the PbS and Pt/PbS nanoparticles. The results reveal that the structure of the PbS and Pt/PbS nanoparticles are mostly composed of PbS, which indicates that the deposition of Pt over the PbS has no significant effect on the structure of PbS. Additionally, no peaks for Pt or Pt_2O appeared for the Pt/PbS pattern, which indicates that Pt is well dispersed on the PbS. The deposition of Pt affects only the crystallization of PbS, which broadened the PbS peaks and decreased their intensity as the Pt wt% increased (Fig. 1). Therefore, as the wt% of Pt decreased, the particle size of PbS decreased.

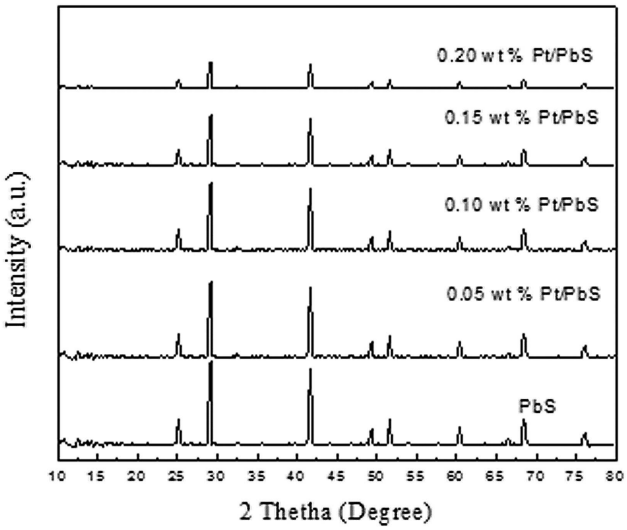

Figure 1. XRD patterns of PbS and Pt/PbS nanoparticles.

XPS measurements were performed to determine the nature of the Pt introduced into the PbS suspension. XPS for 1.5 wt% Pt/PbS is shown in Fig. 2. The results reveal that the peaks assigned to Pt, which indicate the formation of nanoscale Pt metal, appeared at approximately 70.4 and 74 eV.

Figure 3 shows the TEM images of the Pt/PbS nanoparticles. The results revealed that the particle size of the PbS nanoparticles decreased as the wt% of Pt increased, whereas the particle size of the Pt on the PbS increased as the wt% of the Pt increased. Additionally, the increased wt% of Pt from 0.05 to 0.15 increased the homogeneity of the Pt on the PbS. However, above 0.15 wt% of Pt, the homogeneity of the Pt decreased, which means that the optimum value for the wt % of Pt is 0.15.

Table 1. Chromatographic conditions applied for the photocatalytic oxidation of thiophene

	Oxidation of thiophene
Oven	50°C for 5 min → 200°C with 10°C/min
Detector	Type: FED
	Heater: 300°C
	H_2 flow: 150 mL/min
	Air flow: 110 mL/min
	Makeup flow: 25 mL/min
Injection	Heater: 250°C
	Pressure: 13.762 psi
	Total flow: 41.384 mL/min
	Septum purge flow: 3 mL/min
	Mode: split with ratio (10:1)
Column	(30 m × 0.32 μm × 0.25 μm)

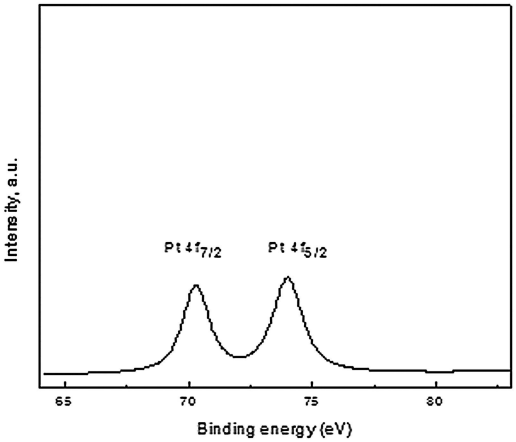

Figure 2. XPS for Pt species of 1.5 wt% Pt/PbS nanoparticles.

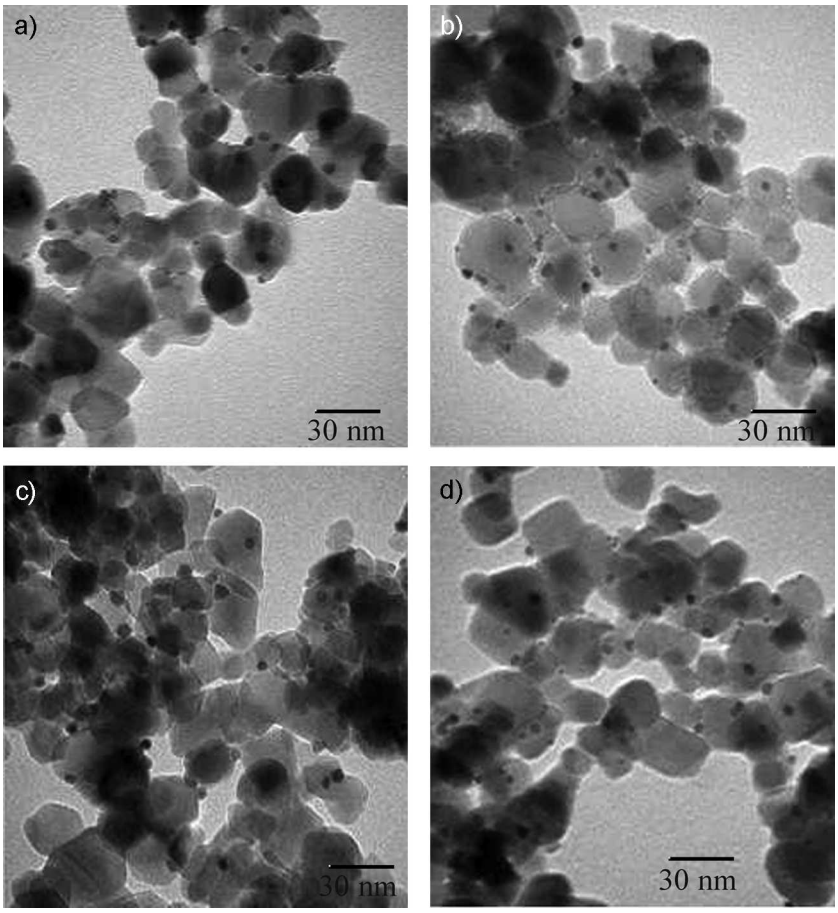

Figure 3. TEM images of Pt/PbS nanoparticles, for which the wt% of Pt is 0.05 (A), 0.10 (B), 0.15 (C), and 0.20 (D).

Table 2. Texture parameters of the PbS and Pt/PbS nanoparticles

Sample	S_{BET} (m^2/g)	S_t (m^2/g)	S_{mic} (cm^2/g)	S_{ext} (cm^2/g)	V_p (cm^3/g)	V_{micro} (cm^3/g)	V_{meso} (cm^3/g)	r (Å)
PbS	19.00	20.00	9.00	10.00	0.112	0.081	0.031	38.00
0.05 wt % Pt/PbS	17.00	18.00	8.00	9.00	0.094	0.066	0.028	42.00
0.10 wt % Pt/ PbS	15.00	16.00	7.00	8.00	0.086	0.060	0.026	46.00
0.15 wt % Pt/PbS	13.00	14.00	600	7.00	0.073	0.050	0.023	48.00
0.20 wt % Pt/PbS	11.00	13.00	5.00	6.00	0.068	0.047	0.021	52.00

S_{BET}, BET-surface area; S_t, surface area derived from V_{l-t} plots; S_{mic}, surface area of micropores; S_{ext}, external surface area; V_p, total pore volume; V_{mic}, pore volume of micropores; V_{mes}, pore volume of mesopores; r, mean pore radius.

3.2 Surface-area analysis

The Brunauer–Emmett–Teller (BET) specific surface areas of PbS and Pt/PbS nanoparticles were determined. The S_{BET} values for PbS, 0.05 wt% Pt/PbS, 0.10 wt% Pt/PbS, 0.15 wt% Pt/PbS, and 0.20 wt% Pt/PbS were 19, 17, 15, 13, and 11 m^2/g, respectively. Table 2 shows the surface-area parameters and the data calculated from the *t*-plot for the PbS and Pt/PbS nanoparticles. The total pore volume of the Pt/PbS nanoparticles was lower than that of the PbS, due to the deposition of Pt onto the PbS surface causing the blockage of pores of the PbS nanoparticle.

3.3 Optical characterization

Figure 4 shows the UV–Vis diffuse reflectance spectra of the PbS and Pt/PbS nanoparticles. The results reveal that the deposition of

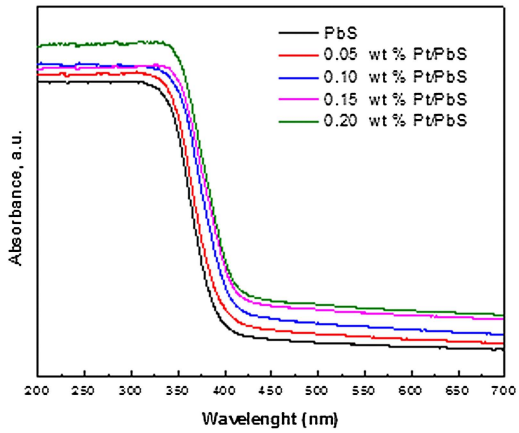

Figure 4. UV–Vis absorption spectra of PbS and Pt/PbS nanoparticles.

CLEAN Soil Air Water

Table 3. Band-gap energies of the PbS and Pt/PbS nanoparticles

Sample	Band-gap energy (eV)
PbS	3.05
0.05 wt% Pt/PbS	2.96
0.10 wt% Pt/PbS	2.85
0.15 wt% Pt/PbS	2.80
0.20 wt% Pt/PbS	2.78

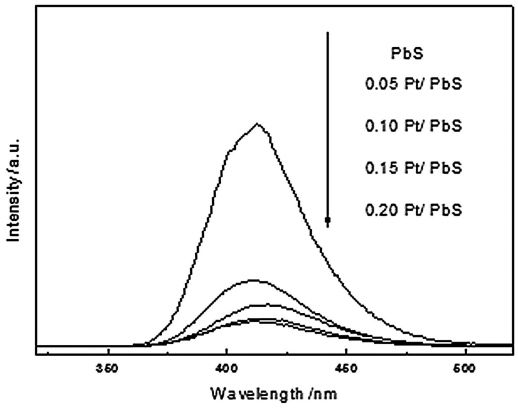

Figure 5. PL spectra of PbS and Pt/PbS nanoparticles.

Pt onto PbS caused a red shift from 407 to 445 nm for the PbS and the 0.2 wt% Pt/PbS nanoparticles, respectively. Table 3 shows the direct band-gap energies for PbS and Pt/PbS, which are calculated from Fig. 4 by the method described in a previous work [18]. The results reveal that the band gap of PbS, 0.05 wt% Pt/PbS, 0.10 wt% Pt/PbS, 0.15 wt% Pt/PbS, and 0.20 wt% Pt/PbS were 3.05, 2.96, 2.85, 2.80, and 2.78 eV, respectively.

Figure 5 shows the PL spectra of the PbS and Pt/PbS nanoparticles. The results reveal that the increased wt% of Pt decreased the PL intensity of PbS, which means that Pt acts as a trapping site. Therefore, the deposition of Pt onto PbS lead to an increased e−h recombination lifetime and an increased photocatalytic activity.

3.4 Photocatalytic activity

3.4.1 Effect of wt% of Pt on the photocatalytic activity of PbS for the oxidation of thiophene

Figure 6 shows the effect of the wt% of Pt on the photocatalytic activity of PbS for the oxidation of thiophene. The experiment was performed under the following conditions: 0.6 g of the photocatalyst, 600 ppm of thiophene, and 500 mL of the thiophene solution. The results reveal that the parent photocatalyst (PbS) has no photocatalytic activity under visible light because it absorbs in the UV region and the experiment is performed under visible light. Additionally, we noticed that the deposition of Pt onto PbS leads to increased photocatalytic activity in the following order: PbS < 0.05 wt% Pt/PbS < 0.1 wt% Pt/PbS < 0.20 wt% Pt/PbS < 0.15 wt% Pt/ PbS. Therefore, the 0.15 wt% Pt/PbS has the highest photocatalytic activity.

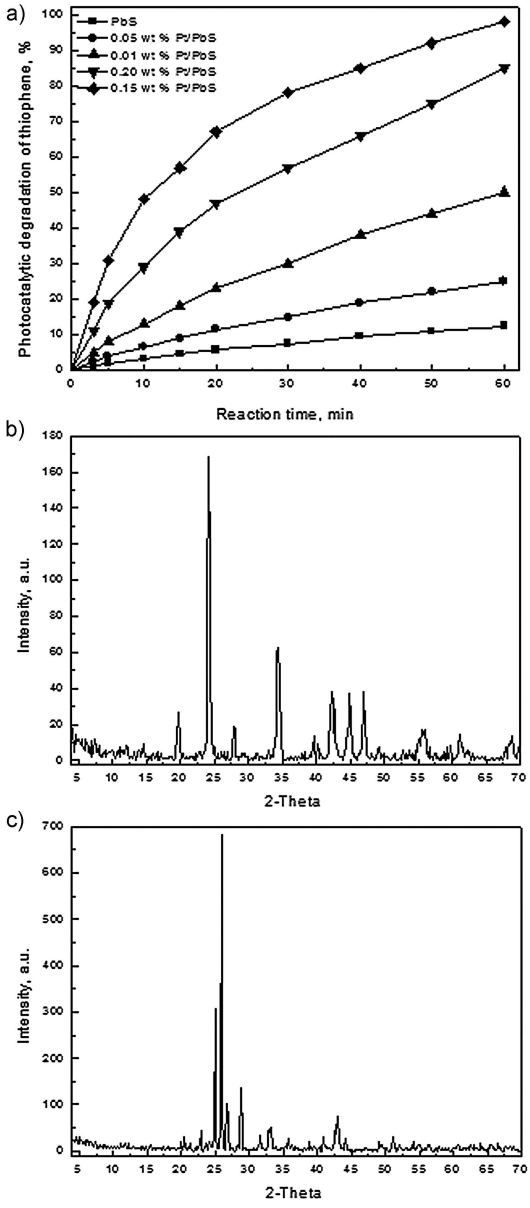

Figure 6. (a) Effect of various catalysts on the photocatalytic oxidation of thiophene under visible-light irradiation, (b) XRD pattern of precipitate 1, and (c) XRD pattern of precipitate 2.

To examine the photoproducts, the gas was introduced into a 0.2 M aqueous NaOH solution for further analysis. After the addition of a 0.2 M aqueous $Ba(NO_3)_2$ solution, a white precipitate was obtained and denoted as precipitate 1. The white precipitate $BaCO_3$ was produced as shown in Fig. 6b. This result indicates that CO_2 is one product of photocatalytic oxidation of thiophene. When an attempt was made to dissolve precipitate 1 in aqueous HNO_3, a portion of white precipitate could not be dissolved and was denoted as precipitate 2. The XRD pattern of precipitate 2 can be readily assigned to $BaSO_4$, as shown in Fig. 6c. This indicates that CO_2 and SO_3 are the main product of photocatalytic oxidation of thiophene as shown in the following equation:

$$\text{Thiophene} + \text{photocatalyst} \rightarrow CO_2 + SO_3 + H_2O \quad (1)$$

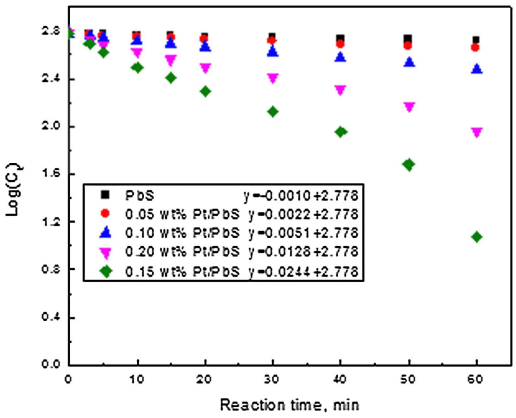

Figure 7. Rate constant for PbS and Pt/PbS nanoparticles.

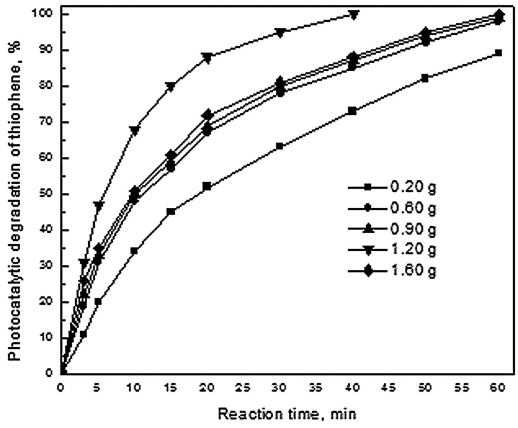

Figure 8. Effect of the loading of 0.15 wt% Pt/PbS on the photocatalytic oxidation of thiophene.

3.4.2 Kinetics of thiophene

The reaction order with respect to thiophene was determined by plotting reaction time *versus* log [thiophene] according to the following equation:

$$\log[C]_t = -kt + \log[C]_o \quad (2)$$

where $[C]_o$ and $[C]_t$ represent the concentration of the substrate in solution at time zero and time t of illumination, respectively, and k represents the apparent rate constant (min^{-1}).

The findings are represented in Fig. 7. The results show that the reaction followed first order kinetics with respect to thiophene and the rate constants were found in the range of 10×10^{-4} to $244 \times 10^{-4}\,min^{-1}$. The first order rate equation for thiophene is given by

$$R = k[\text{thiophene}] \quad (3)$$

3.4.3 Effect of photocatalyst quantity on the photocatalytic activity of PbS for the oxidation of thiophene

Another important factor in the photocatalytic oxidation of thiophene under visible light irradiation is the quantity of the photocatalyst. The quantity of 0.15 wt% Pt/PbS ranged from 0.2 to $1.6\,g\,L^{-1}$ in $1000\,mg\,L^{-1}$ of the selected solutions of thiophene, as shown in Fig. 8. The results reveal that increasing the amount of 0.15 wt% Pt/PbS from 0.2 to $0.9\,g\,L^{-1}$ increases photocatalytic degradation efficiency of thiophene from 89 to 99%, respectively. The reaction time required for the oxidation of thiophene decreased from 60 to 40 min by increasing the amount of 0.15 wt% Pt/PbS from 0.9 to $1.2\,g\,L^{-1}$, respectively. However, increasing the amount of catalyst to >1.2 decreased the photocatalytic degradation of thiophene. This is because increasing the amount of photocatalyst used increases the number of active sites, which increases the photocatalytic activity [31]. However, increasing the amount of photocatalyst above $1.2\,g\,L^{-1}$ blocked the penetration of light to the photocatalyst, and therefore decreased the photocatalytic activity [31]. We found that our 0.15 wt% Pt/PbS photocatalyst has a more effective photocatalytic activity for the oxidation of thiophene than the photocatalyst $Pt(RuO_2)/TiO_2$ [32].

3.4.4 Recycling of the photocatalyst

One of important factors for the commercialization of a photocatalyst is the stability of the photocatalyst. Our 0.15 wt% Pt/PbS photocatalyst was examined for its photocatalytic stability by reusing it six times. The results reveal that after six uses of the 0.15 wt% Pt/PbS photocatalyst, the photocatalytic conversion of thiophene was 100%. Therefore, the photocatalyst was stable and effective for environmental remediation.

4 Conclusions

PbS and Pt/PbS nanoparticles were successfully prepared. The sample with 0.15 wt% Pt/PbS has a high photocatalytic activity for the oxidation of thiophene under visible light, and these results may lead to find potential applications for this material in related fields. UV–Vis spectra reveal that the deposition of Pt onto PbS led to a red shift to a higher wavelength. The use of 0.15 wt% Pt/PbS, 1000 mL of thiophene, and 1.2 g of the catalyst degrades 100% of thiophene under visible light after a reaction time of 40 min. The photocatalytic activity of 0.15 wt% Pt/PbS after use six times remains almost the same, which confirms the photostability of the 0.15 wt% Pt/PbS nanoparticles.

The authors have declared no conflict of interest.

References

[1] Y. Hsien, C. F. Chang, Y. H. Chen, S. Cheng, Photodegradation of Aromatic Pollutants in Water over TiO_2 Supported on Molecular Sieves, *Appl. Catal., B* **2001**, *31*, 241–249.

[2] L. Davydov, E. P. Reddy, P. France, P. G. Smirniotis, Transition-Metal-Substituted Titania-Loaded MCM-41 as Photocatalysts for the Degradation of Aqueous Organics in Visible Light, *J. Catal.* **2001**, *203*, 157–167.

[3] X. M. Gao, F. Fu, L. P. Zhang, W. H. Li, The preparation of Ag–$BiVO_4$ Metal Composite Oxides and Its Application in Efficient Photocatalytic Oxidative Thiophene, *Physica B* **2013**, *419*, 80–85.

CLEAN Soil Air Water

[4] L. Wang, H. Cai, S. Li, N. Mominou, Ultra-Deep Removal of Thiophene Compounds in Diesel Oil over Catalyst TiO_2/Ni-ZSM-5 Assisted by UV Irradiating, *Fuel* **2013**, *105*, 752–756.

[5] F. C. Marques, M. C. Canela, A. M. Stumbo, Use of TiO_2/Cr-MCM-41 Molecular Sieve Irradiated with Visible Light for the Degradation of Thiophene in the Gas Phase, *Catal. Today* **2008**, *133-135*, 594–599.

[6] D. Zhao, F. Li, E. Zhou, Z. Sun, Kinetics and Mechanism of the Photo-oxidation of Thiophene by O_2 Adsorbed on Molecular Sieves, *Chem. Res. Chin. Univ.* **2008**, *24*, 96–100.

[7] R. M. Mohamed, D. L. McKinney, W. M. Sigmund, Enhanced Nanocatalysts, *Mater. Sci. Eng., R* **2012**, *73*, 1–13.

[8] R. M. Mohamed, M. M. Mohamed, Copper(II) Phthalocyanine Immobilized on Alumina and Encapsulated Inside Zeolite X and Their Applications in Photocatalytic Degradation of Cyanide: A Comparative Study, *Appl. Catal., A* **2008**, *340*, 16–24.

[9] Y. D. Shen, T. R. B. Foong, X. Hu, Towards Atomic Level Vanadium Doping of TiO_2 via Liquid-Phase Atomic Layer Deposition, *Appl. Catal., A* **2011**, *409*, 87–90.

[10] R. M. Mohamed, E. S. Baeissa, Mordenite Encapsulated with Pt-TiO_2: Characterization and Applications for Photocatalytic Degradation of Direct Blue Dye, *J. Alloys Compd.* **2013**, *558*, 68–72.

[11] R. M. Mohamed, E. Aazam, Synthesis and Characterization of P-Doped TiO_2 Thin-Films for Photocatalytic Degradation of Butyl Benzyl Phthalate under Visible-Light Irradiation, *Chin. J. Catal.* **2013**, *34*, 1267–1273.

[12] R. M. Mohamed, UV-Assisted Photocatalytic Synthesis of TiO_2-Reduced Graphene Oxide with Enhanced Photocatalytic Activity in Decomposition of Sarin in Gas Phase, *Desalin. Water Treat.* **2012**, *50*, 147–156.

[13] R. M. Mohamed, E. S. Aazam, Preparation and Characterization of Platinum Doped Porous Titania Nanoparticles for Photocatalytic Oxidation of Carbon Monoxide, *J. Alloys Compd.* **2011**, *509*, 10132–10138.

[14] R. M. Mohamed, E. S. Aazam, Characterization and Catalytic Properties of Nano-Sized Au Metal Catalyst on Titanium Containing High Mesoporous Silica (Ti-HMS) Synthesized by Photo-Assisted Deposition and Impregnation Methods, *Int. J. Photoenergy* **2011**, published online. DOI: 10.1155/2011/137328

[15] R. M. Mohamed, I. A. Mkhalid, The Effect of Rare Earth Dopants on the Structure, Surface Texture and Photocatalytic Properties of TiO_2-SiO_2 Prepared by Sol-Gel Method, *J. Alloys Compd.* **2010**, *501*, 143–147.

[16] R. M. Mohamed, I. A. Mkhalid, Characterization and Catalytic Properties of Nano-Sized Ag Metal Catalyst on TiO_2-SiO_2 Synthesized by Photo-Assisted Deposition (PAD) and Impregnation Methods, *J. Alloys Compd.* **2010**, *501*, 301–306.

[17] H. Liu, X. Dong, C. Duan, X. Su, Z. Zhu, Silver-Modified TiO_2 Nanorods with Enhanced Photocatalytic Activity in Visible Light Region, *Ceramics Int.* **2013**, *39*, 789–795.

[18] C. Zhang, L. Ai, L. Li, J. Jiang, One-Pot Solvothermal Synthesis of Highly Efficient, Daylight Active and Recyclable Ag/AgBr Coupled Photocatalysts with Synergistic Dual Photoexcitation, *J. Alloys Compd.* **2014**, *582*, 576–582.

[19] V. Iliev, D. Tomova, S. Rakovsky, A. Eliyas, G. Li Puma, Enhancement of Photocatalytic Oxidation of Oxalic Acid by Gold Modified WO_3/TiO_2 Photocatalysts under UV and Visible Light Irradiation, *J. Mol. Catal. A: Chem.* **2010**, *327*, 51–57.

[20] Y. Sun, B. Zhou, Single-Crystalline Ag_2S Hollow Nanohexagons and Their Assembly into Ordered Arrays, *Mater. Lett.* **2010**, *64*, 1347–1349.

[21] Y. Sun, B. Zhou, P. Gao, H. Mu, L. Chu, Single-Crystalline Ag_2S Hollow Nanoparticles and Their Ordered Arrays, *J. Alloys Compd.* **2010**, *490*, L48–L51.

[22] S. Hull, D. A. Keen, D. S. Sivia, P. A. Madden, M. Wilson, The Effect of Morphology on the Temperature-Dependent Photoluminescence Quantum Efficiency of the Conjugated Polymer Poly(9,9-dioctyl-fluorene), *J. Phys. Condens. Matter.* **2002**, *14*, 9–17.

[23] T. Minami, Recent Progress in Superionic Conducting Glasses, *J. Non-Cryst. Solids* **1987**, *95*, 107–118.

[24] Y. P. Sun, J. E. Riggs, H. W. Rollins, R. Guduru, Strong Optical Limiting of Silver-Containing Nanocrystalline Particles in Stable Suspensions, *J. Phys. Chem. B* **1999**, *103*, 77–82.

[25] J. C. Liu, P. Raveendran, Z. Shervani, Y. Ikushima, Synthesis of Ag_2S Quantum Dots in Water-in-CO_2 Microemulsions, *Chem. Commun.* **2004**, 2582–2583.

[26] L. Armelao, R. Bertoncello, E. Cattaruzza, S. Gialanella, S. Gross, G. Mattei, P. Mazzoldi, et al., Chemical and Physical Routes for Composite Materials Synthesis: Ag and Ag_2S Nanoparticles in Silica Glass by Sol-Gel and Ion Implantation Techniques, *J. Mater. Chem.* **2002**, *12*, 2401–2407.

[27] J. P. Xiao, Y. Xie, R. Tang, W. Luo, Template-Based Synthesis of Nanoscale Ag_2E (E = S, Se) Dendrites, *J. Mater. Chem.* **2002**, *12*, 1148–1151.

[28] R. V. Kumar, O. Palchik, Y. Koltypin, Y. Diamant, A. Gedanken, Sonochemical Synthesis and Characterization of Ag_2S/PVA and CuS/PVA Nanocomposite, *Ultrason. Sonochem.* **2002**, *9*, 65–70.

[29] M. Chen, Y. Xie, H. Y. Chen, Z. P. Qiao, Y. T. Qian, Preparation and Characterization of Metal Sulfides in Ethylenediamine under Ambient Conditions through a γ-Irradiation Route, *J. Colloid Interface Sci.* **2001**, *237*, 47–53.

[30] W. P. Lim, Z. Zhang, H. Y. Low, W. S. Chin, Preparation of Ag_2S Nanocrystals of Predictable Shape and Size, *Angew. Chem. Int. Ed.* **2004**, *43*, 5685–5689.

[31] J. Nishio, M. Tokumura, H. T. Znad, Y. Kawase, Photocatalytic Decolorization of Azo-Dye with Zinc Oxide Powder in an External UV Light Irradiation Slurry Photoreactor, *J. Hazard. Mater.* **2006**, *138*, 106–115.

[32] F. Lin, Y. Zhang, L. Wang, Y. Zhang, D. Wang, M. Yang, J. Yang, et al., Highly Efficient Photocatalytic Oxidation of Sulfur-containing Organic Compounds and Dyes on TiO_2 with Dual Cocatalysts Pt and RuO_2, *Appl. Catal., A* **2012**, *127*, 363–370.

